RSC Advances

PAPER

View Article Online
View Journal | View Issue

Cite this: *RSC Adv.*, 2020, **10**, 3137

Gum acacia-based silver nanoparticles as a highly selective and sensitive dual nanosensor for Hg(II) and fluorescence turn-off sensor for S^{2-} and malachite green detection†

Ambreen Abbasi, Summaiya Hanif and Mohammad Shakir *

Received 10th December 2019
Accepted 28th December 2019

DOI: 10.1039/c9ra10372d

rsc.li/rsc-advances

A facile and green method was adopted to synthesize highly selective gum acacia-mediated silver nanoparticles as dual sensor (fluorescence turn-on and colorimetric) for Hg(II) and fluorescence turn-off sensor for S^{2-} and malachite green. The mechanism proposed for a dual response towards Hg(II) is the redox reaction between Ag(0) and Hg(II), resulting in the formation of Ag(I) and Hg(0) and electron transfer from gum acacia to Ag(I), which further leads to the formation of an Ag@Hg nanoalloy. The enhanced fluorescence signal was quenched selectively by S^{2-} owing to the formation of Ag_2S and HgS. The reported nanosensor was found to be useful for sensing malachite green *via* the inner filter effect. The linear ranges were 3 nmol L^{-1} to 13 μmol L^{-1} for Hg(II), 3–170 μmol L^{-1} for S^{2-} and 7–80 μmol L^{-1} for malachite green, and the corresponding detection limits were 2.1 nmol L^{-1} for Hg(II), 1.3 μmol L^{-1} for S^{2-} and 1.6 μmol L^{-1} for malachite green.

1. Introduction

Controlling the levels of hazardous metals is vital due to their adverse effects on human health and the environment.[1] Elemental (Hg(0)), inorganic mercurous and mercuric forms (Hg(I) and Hg(II), respectively) and organic alkyl mercury are the four chemical forms in which mercury exists.[2] Hg(II) emission from several sources such as power plants, fossil fuels, forest fires, burning of municipal and medical wastes and discharge from mining and paper industries are significant causes of Hg(II) contamination.[3] In humans, mercury poisoning can lead to hearing impairment, muscle weakness, skin rashes, imperfect eyesight, difficulty in speech, damage to the neurological, gastrointestinal and renal organ systems and Minamata disease.[4] Therefore, these detrimental environmental and health effects of Hg(II) have encouraged researchers to design effective methods for the selective and sensitive detection of mercury to get a clear idea of its distribution and pollution potential. To resolve this issue, various sophisticated analytical instrumental methods such as cold vapor technique with atomic absorption spectrometry,[5] high-performance liquid chromatography coupled with UV-Vis or fluorescence spectroscopy,[6] and inductively coupled plasma atomic emission and mass spectroscopy[5] have been put forward for the qualitative or quantitative detection of mercury. However, these instrumental techniques pose several limitations in practical use, some of which are high-time consumption, complex procedures, costly equipment, and incompatibility with aqueous environments.[7] To overcome these disadvantages, researchers have developed optical methods such as colorimetric, fluorescence, surface plasmon resonance, and surface-enhanced Raman scattering for the detection of mercury.[8] Fluorescence spectroscopy and colorimetric method have surpassed the above-mentioned methods owing to their high sensitivity and selectivity, fast analysis, and less complicated experimental procedures.[9,10]

Noble metal nanoparticles such as gold and silver have aroused a great deal of recognition because of the optical phenomenon called 'Surface Plasmon Resonance' exhibited by them.[11–13] Silver nanoparticle (AgNP)-based optical sensors are considered to be more efficient and sensitive compared to gold nanoparticle-based sensors because of the higher visible region molar extinction coefficient of silver nanoparticles (more than 100 fold).[14] AgNPs are known to be photostable and are less likely to undergo photobleaching, thereby allowing these nanoparticles to be utilized as optical sensors for ultrasensitive mercury detection.[15–17]

Hazardous sulfide ions (S^{2-}) have a widespread distribution in both natural and wastewater and are frequently found in industrial areas, such as food processing units, petroleum refineries, and paper and pulp production plants.[18] Sulfide in its protonated state becomes even more toxic and poisonous as it turns into bisulfide and gaseous hydrogen sulfide.[19] Chronic subjection to protonated sulfide has been associated with

Division of Inorganic Chemistry, Department of Chemistry, Aligarh Muslim University, Aligarh 202002, India. E-mail: shakir078@yahoo.com; Tel: +919837430035

† Electronic supplementary information (ESI) available. See DOI: 10.1039/c9ra10372d

numerous diseases such as Down's syndrome, Alzheimer's disease, and liver cirrhosis.[20] Thus, there is an urgent need to monitor high levels of sulfide in biological and environmental samples. Several analytical techniques, such as chemiluminescence,[21] colorimetry,[22] polarography,[23] spectroscopy[24] and fluorometry,[25] have been adopted to overcome this problem. Amongst all these methods, fluorescence assay shows predominance over the other processes owing to its high sensitivity and selectivity, quick detection, and ease of operation. In particular, newly developed fluorescent nanomaterials with outstanding photophysical properties and excellent biocompatibility present new opportunities for constructing novel sulfide fluorescence analysis methods.[26]

In the dyestuff industry, malachite green (MG) has been classified as a triarylmethane dye. MG's full antimicrobial spectrum has made it an efficient antiparasitic agent and fungicide in the aquaculture industry.[27] Many studies have proven malachite green's environmental persistence and acute toxicity to terrestrial and aquatic animals, and also, its carcinogenic, teratogenic, and mutagenic effects on the human body.[28] Even though many countries have banned the use of malachite green in aquaculture and food industry, malachite green has been lawlessly used owing to its full antimicrobial spectrum, low cost and availability. Thus, it is of utmost importance to design sensors for the detection of malachite green in environmental samples.

Encouraged by the above findings, the focus of the present study is to establish a new and straightforward dual nanosensor for Hg(II) and fluorescence turn-off sensor for sulfide ions and malachite green. The as-prepared nanoparticles were proposed to form the Ag@Hg nanoalloy, which were responsible for the color change from yellow to colorless and for the increase in the fluorescence intensity compared to that of AgNPs in the absence of Hg(II). The fluorescent GA-AgNPs and Hg(II) ensemble was further utilized for fluorescence sensing of sulfide by making use of the low K_{sp} values of Ag_2S (6.3×10^{-50})[29] and HgS (1×10^{-54}). Further, the nanosensor was capable of sensing malachite green *via* the inner filter effect. Our developed nanosensor was found to be extremely stable, displaying a slight decrease in absorbance and fluorescence intensity after ten months of storage in the dark under room temperature conditions. We have also successfully employed our synthesized nanosensor to detect Hg(II), S^{2-} ions, and MG in real water samples such as tap water, packaged drinking water, and bore-well water.

2. Experimental

See ESI S1.†

3. Results and discussion

The AgNPs were synthesized using gum acacia as both reducing and stabilizing agents. The as-prepared colloidal solution of AgNPs exhibited a yellow color. Various spectroscopic and microscopic techniques were used to characterize the as-prepared nanoparticles, and their dual response, *i.e.*, both colorimetric and fluorescence responses towards Hg(II) ions were studied. The nanosensor was further used to detect sulfide ions *via* fluorescence turn-off mechanism and MG *via* the inner filter effect. Fig. 1S† shows the fluorescence spectrum of GA-AgNPs in an aqueous solution. The fluorescence intensity of the as-synthesized GA-AgNPs did not exhibit any significant change after ten months of storage at room temperature conditions in the dark, thereby proving the stability of the as-synthesized nanoparticles. At 300 nm, excitation GA-AgNPs exhibited an emission band in the visible region centered at 568 nm. The Stokes shift was found to be larger than that of fluorescent proteins and organic dyes, which are known to be the most conventional fluorophores, thereby making GA-AgNPs advantageous in various analytical applications. The emission peak of GA-AgNPs shifted to a higher wavelength (Fig. 2S†) with an increase in the excitation wavelength; such an observation is not uncommon in the case of AgNPs,[30] which could be attributed to different particle sizes.

3.1. FT-IR spectroscopy

FT-IR spectroscopy was used to ascertain the surface chemistry of GA-AgNPs. Fig. 1 displays the respective spectra of pure gum acacia (GA), GA-AgNPs, and GA-AgNPs in the presence of Hg(II) ions. The major peaks of GA shifted from 3406 cm^{-1} (O–H stretching), 2931 cm^{-1} (C–H stretching), 1728 cm^{-1} (C=O stretching), 1632 cm^{-1} (C=O stretching), and 1067 cm^{-1} (C–OH stretching) to 3424 cm^{-1}, 2920 cm^{-1}, 1722 cm^{-1}, 1626 cm^{-1} and 1061 cm^{-1}, respectively.[31] These data supported the capping of silver nanoparticles with gum acacia with the involvement of –COOH and –OH groups. In the presence of Hg(II) ions, bands corresponding to (O–H stretching), (C–H stretching), (C=O stretching) and (C–OH stretching) shifted further to 3436 cm^{-1}, 2922 cm^{-1}, 1734 cm^{-1}, 1618 cm^{-1}, and 1049 cm^{-1}, respectively, and a reduction in the intensity of the respective bands was also observed, suggesting the coordination of –COOH and –OH groups of gum acacia with Hg(II) ions forming gum acacia and Hg(II) complex and also some electronic changes.

3.2. SEM and EDX analysis

Fig. 2A–C give the SEM and EDX images of GA-AgNPs, GA-AgNPs in the presence of Hg(II) and, GA-AgNPs in the presence of Hg(II) and S^{2-} ions.

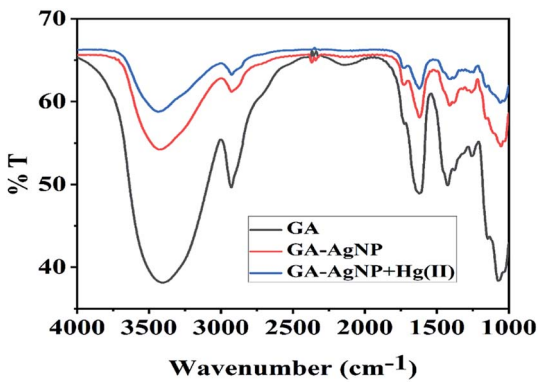

Fig. 1 The FT-IR spectrum of Gum Acacia (GA) (black), GA-capped AgNPs (red), and GA-capped AgNPs in the presence of 100 nmol L^{-1} Hg(II) ions (blue).

3.3. Confocal imaging

The confocal image of the as-synthesized nanosensor is given in Fig. 3S.† The unlabeled nanosensor exhibited orange-red fluorescence.

3.4. TEM analysis

Fig. 3A shows a typical TEM image of the as-synthesized nanosensor. It is clear from the image that majority of the particles are spherical with an average diameter of 1.5 nm.

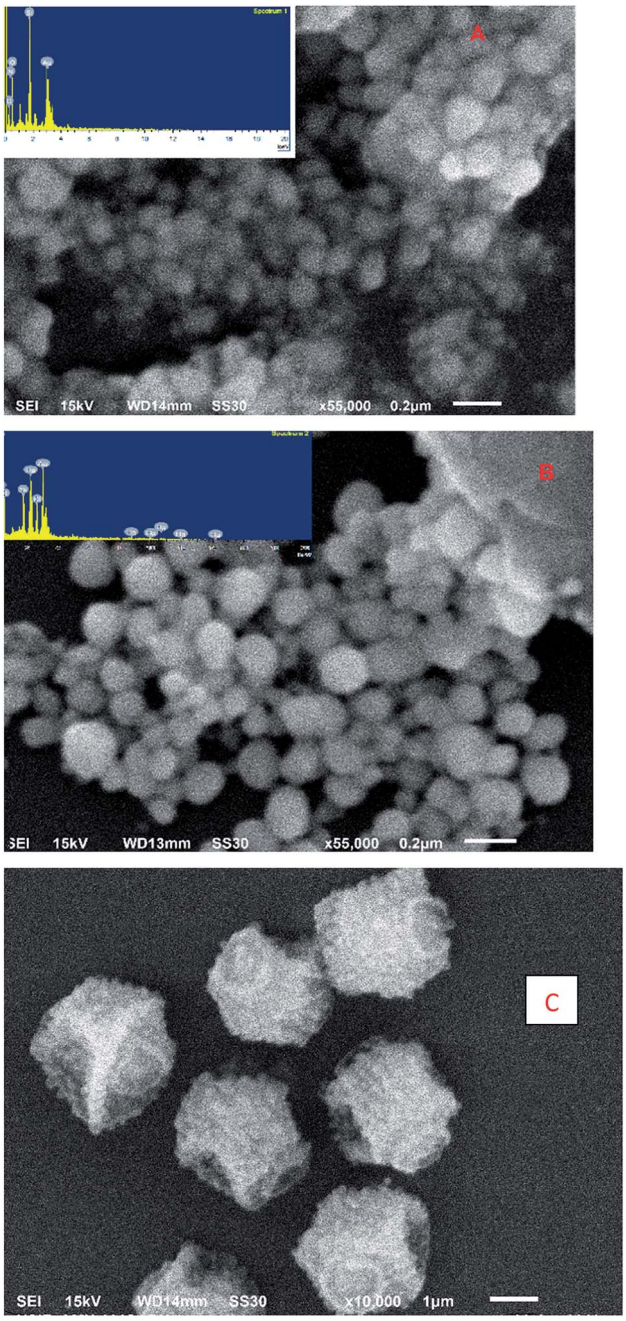

Fig. 2 SEM images of GA-AgNPs (A), GA-AgNPs in the presence of 100 nmol L^{-1} Hg(II) (B) and GA-AgNPs in the presence of 100 nmol L^{-1} and 30 μmol L^{-1} S^{2-} ions (C). Insets of (A) and (B) give the EDX image.

Fig. 3B shows the TEM image of the nanosensor in the presence of Hg(II) ions. It is clear from the image that the nanoparticles are spherical with an average diameter of 21 nm.

3.5. XRD analysis

The XRD diffraction patterns of GA-AgNPs in the absence and presence of 100 nmol L^{-1} Hg(II) ions are shown in Fig. 4S(a) and (b).† The XRD pattern of GA-AgNPs alone shows diffraction peaks at 38.28° and 44.44°, corresponding to the (111) and (200) planes of the FCC crystal structure, respectively.

The XRD pattern of GA-AgNPs in the presence of Hg(II) ions matched well with the pattern reported for Ag@Hg nanoalloys in the literature.[32]

3.6. pH effect

To ascertain the influence of pH on the sensing behavior of GA-AgNPs, the pH was varied with 0.1 mol L^{-1} HCl and NaOH solutions. We have studied the fluorescence response of our nanosensor alone and with Hg(II) ions. For GA-AgNPs alone (Fig. 5S†), no significant variation in the pH range 4–11 was observed. With the addition of Hg(II) ions, the nanosensor exhibited a fluorescence turn-on behavior in the pH range 4–11 with maximum enhancement at neutral pH (Fig. 5S†). Therefore, neutral pH was selected for the entire study.

3.7. The fluorescence response of GA-AgNPs towards Hg(II) ions

The fluorescence response of the nanosensor to other metal ions at neutral pH was studied to ascertain the selectivity toward Hg(II) ions. Out of all the metal ions studied, only Hg(II) ions induced a fluorescence enhancement, whereas the other competing metal ions such as K^{+}, Na^{+}, Ca^{2+}, Mg^{2+}, Ba^{2+}, Mn^{2+}, Co^{2+}, Cr^{3+}, Fe^{2+}, Fe^{3+}, Cu^{2+}, Zn^{2+}, Cd^{2+}, Ni^{2+}, Al^{3+}, and Pb^{2+} even in millimolar concentrations could not induce any significant change in the fluorescence intensity of GA-AgNPs (Fig. 6S†). Furthermore, the same response was obtained on adding Hg(II) ions to a mixture of competing metal ions (20 μmol L^{-1}) and Hg(II) ions alone (Fig. 6S†). These results indicate that our developed nanosensor is highly selective towards Hg(II) ions.

Fig. 4 reveals that the fluorescence intensity of the nanosensor is sensitive to the concentration of Hg(II) ions in the range of 3 nmol L^{-1} to 13 μmol L^{-1} M, and an increase in the Hg(II) levels leads to an enhancement in the fluorescence intensity. The linear regression relationship ($y = 2 \times 10^{7}x + 0.3075$, $R^2 = 0.989$) between the fluorescence intensity and the concentration of Hg(II) ions was used to determine the limit of detection, which was found to be 2.1 nmol L^{-1}. The LOD obtained for our nanosensor was found to be much lower than the maximum contamination level of Hg(II) in drinking water (10 nmol L^{-1}) as defined by the U.S Environmental Protection Agency (EPA).

3.8. Fluorescence sensing of S^{2-} ions

High selectivity is the principal criterion in practical applications; therefore, the selectivity of the GA-AgNPs–Hg(II) ensemble towards S^{2-} ions and other anions such as Cl^{-}, ClO_4^{-}, NO_3^{-}, NO_2^{-}, SO_4^{2-},

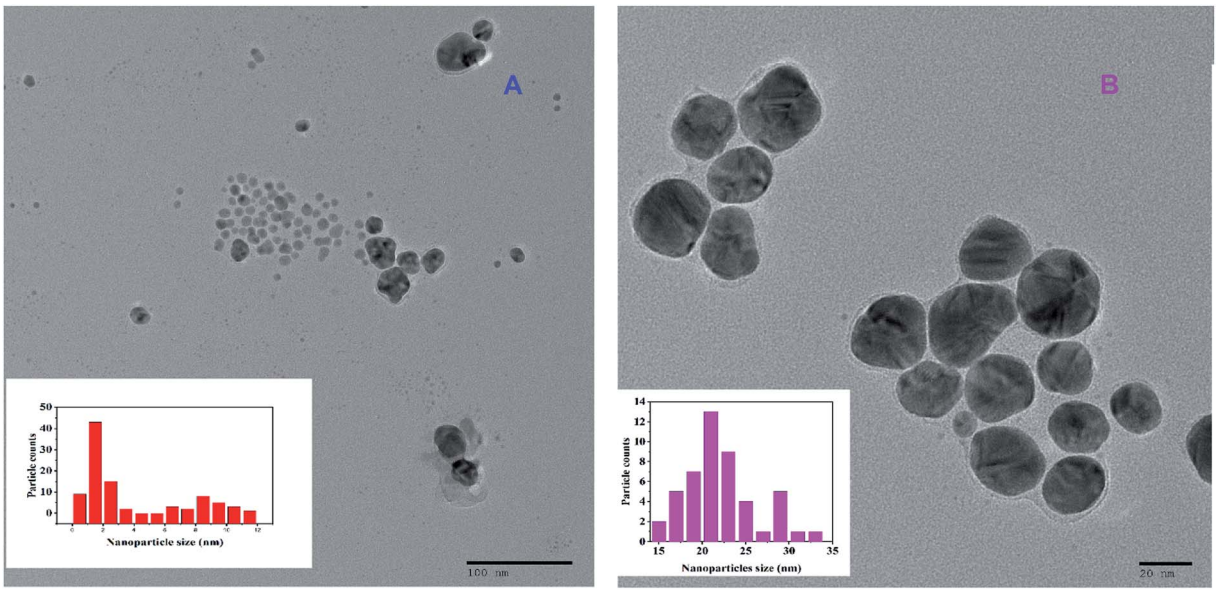

Fig. 3 TEM image of GA-AgNPs alone (A) and GA-AgNPs in the presence of 100 nmol L^{-1} Hg(II) ions (B). Insets give the size distribution histogram.

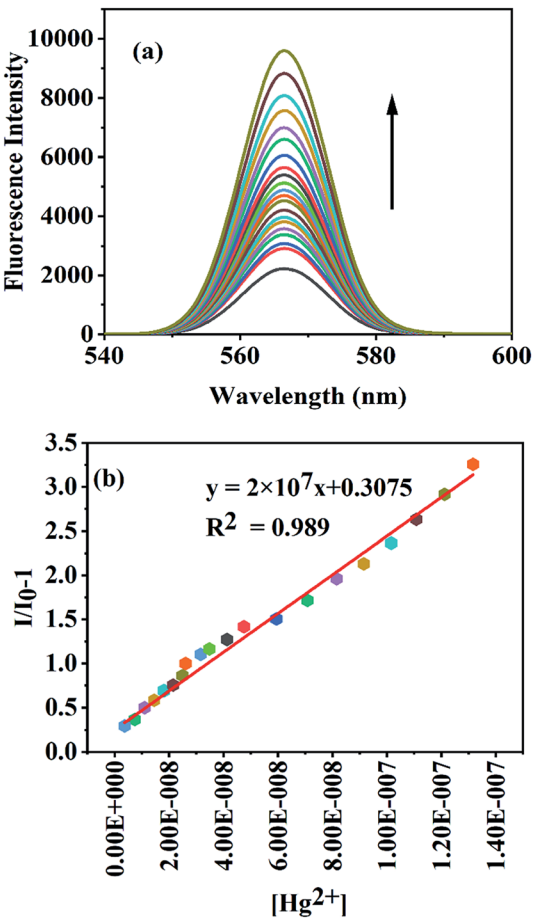

Fig. 4 (a) Fluorescence turn-on response of GA-AgNPs in the presence of an increasing concentration of Hg(II) [3 nmol L^{-1} to 13 μmol L^{-1}]; (b) calibration curve showing fluorescence enhancement linearity.

Br^-, BrO_3^-, CrO_4^{2-}, I^-, IO_3^-, IO_4^-, SCN^-, PO_4^{3-}, CO_3^{2-}, CH_3COO^-, and F^- was studied. Fig. 7S† shows that only S^{2-} ion is able to quench the enhanced fluorescence of the GA-AgNP–Hg(II) ensemble, and the other anions do not produce any noticeable changes in the fluorescence intensity of the GA-AgNP–Hg(II) ensemble, signifying that the observed fluorescence quenching of the GA-AgNP–Hg(II) group was highly specific to S^{2-} ions.

To further evaluate the workability of our approach for quantitative analysis, fluorescence spectroscopy was used to investigate the responses of the GA-AgNP–Hg(II) ensemble toward different S^{2-} concentrations (3–170 μmol L^{-1}). As shown in Fig. 5, the fluorescence intensity of the GA-AgNP–Hg(II) ensemble gradually decreased as the S^{2-} concentration increased. The linear regression relationship ($y = 19\,808x + 1.039$, $R^2 = 0.992$) between the relative fluorescence intensity and the concentration of S^{2-} ion over the range from 3–170 μmol L^{-1} at 568 nm was used to determine the limit of detection, which was found to be 1.3 μmol L^{-1}.

3.9. Fluorescence response of GA-AgNPs towards MG

Fig. 6 reveals that the fluorescence intensity of the nanosensor is sensitive to the concentration of MG, and shows a gradual decrease in the fluorescence intensity with the increase in the MG concentration in the range 7–130 μmol L^{-1}. The linear regression relationship ($y = 34\,326x + 0.7581$, $R^2 = 0.997$) between the relative fluorescence intensity and the concentration of MG over the range from 7–80 μmol L^{-1} at 568 nm was used to determine the limit of detection, which was found to be 1.6 μmol L^{-1}.

3.10. The mechanism for the colorimetric and fluorescence turn-on response of GA-AgNPs to Hg(II) ions and turn-off response to S^{2-} ions

The vivid yellow color of the diluted colloidal solution of AgNPs changed to colorless with the addition of Hg(II) ions (Fig. 8S†),

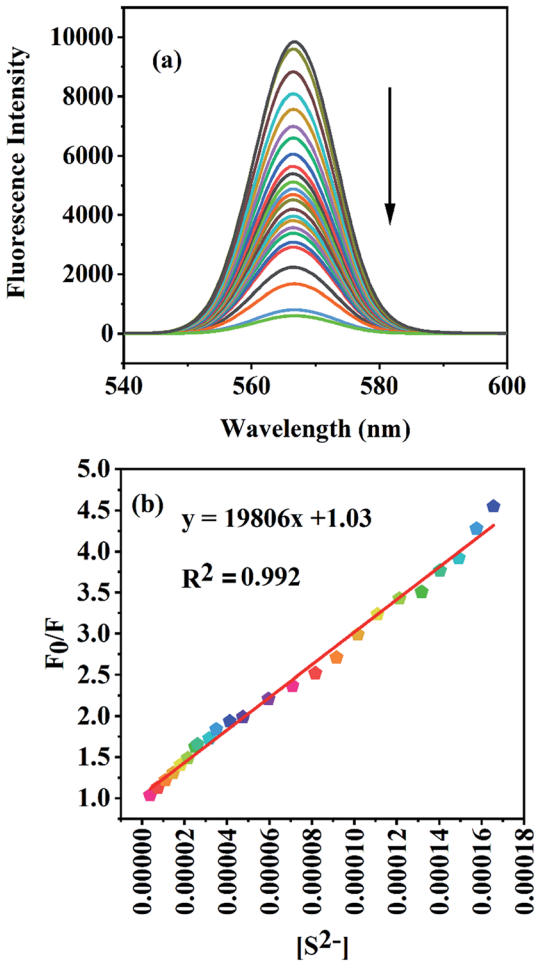

Fig. 5 (a) Fluorescence turn-off response of the GA-AgNPs–Hg(II) ensemble in the presence of an increasing concentration of S^{2-} [3–170 μmol L^{-1}]; (b) the relative fluorescence intensity at 567 nm against S^{2-}.

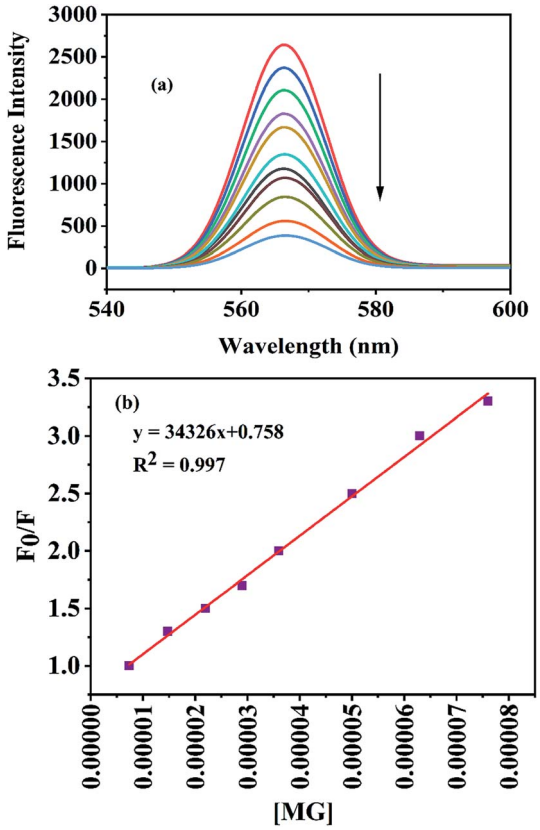

Fig. 6 (a) Fluorescence turn-off response of GA-AgNPs in the presence of an increasing concentration of MG [7–130 μmol L^{-1}]; (b) the relative fluorescence intensity at 567 nm against MG in the concentration range 7–80 μmol L^{-1}.

and the surface plasmon resonance peak of AgNPs exhibited a blue shift (Fig. 9S†), which could be attributed to the oxidation of AgNPs to Ag(I) due to the redox reaction between zerovalent Ag and Hg(II) ions, which subsequently lead to the formation of the Ag@Hg nanoalloy.[1]

The possible mechanism for the fluorescence enhancement on the addition of Hg(II) ions is as follows: initially, Hg(II) coordinates with gum acacia through –COOH and –OH groups, as supported by the FT-IR analysis, leading to the formation of Hg–gum acacia complex. With an increase in concentration, Hg(II) ions rapidly adsorb on the surface of the nanoparticles, after which a redox reaction occurs between Ag(0) and Hg(II) forming Ag(I) and Hg(0). The Ag(I) is converted to Ag(0) *via* electron transfer from gum acacia to Ag(I), thereby bringing about an electronic change in gum acacia, which could lead to the fluorescence enhancement. This electron transfer from gum acacia to Ag(I) gained support from the proposed synthetic procedure, where no additional reducing agent was used to prepare the nanoparticles.

The formation of nanoalloys was supported by EDX analysis, XRD study, and an increase in the size of the nanoparticles suggested by the TEM analysis. The increment in size was due to the well-known "swelling effect",[33] which occurs due to the diffusion of Hg atoms, which increases the total atoms per nanoparticles.

The quenching of fluorescence on the addition of sulfide ions could be due to the displacement of gum acacia on the surface of the nanoparticles by sulfide ions because of the higher affinity of silver and mercury for sulphide ions, leading to the formation of Ag_2S and HgS owing to the low K_{sp} values of Ag_2S (1×10^{-50}) and HgS (1×10^{-54}).

3.11. The mechanism for the detection of MG

The UV-Vis absorption band of MG shows spectral overlaps with the emission band of GA-AgNPs (Fig. 10S†). The possible mechanisms for quenching are fluorescence resonance energy transfer (FRET) or the inner filter effect (IFE), which mainly arises due to the absorption of the excitation and emission light of the fluorophore by the absorber molecule.[34] On gradual addition of MG into a dilute colloidal solution of GA-AgNPs, no change in the absorption spectrum of GA-AgNPs was observed (Fig. 11S†). Instead, there was the appearance of absorption bands of MG, which increased in intensity with the increase in

Table 1 Performance of GA-AgNPs as a probe for the detection of Hg^{2+}, S^{2-} and MG with other reported NP-based methods

NPs	Linear range (M)	LOD (M)	Analytical technique	Analyte detected	Reference
Na-CysC-AgNPs	$5–50 \times 10^{-9}$	8×10^{-9}	UV-Vis	Hg^{2+}	1
Gln-His-AgNPs	40×10^{-9} to 1.5×10^{-6}	5×10^{-9}	UV-Vis	Hg^{2+}	37
GK-AgNPs	$50–900 \times 10^{-9}$	50×10^{-9}	UV-Vis	Hg^{2+}	2
Syzygium aqueum AgNPs	$0.5–100 \times 10^{-6}$	8.5×10^{-7}	UV-Vis	Hg^{2+}	38
Gallotannin-AgNPs	$0.1–1 \times 10^{-9}$	0.037×10^{-9}	UV-Vis	Hg^{2+}	39
Oligonucleotide-AgNCs	40×10^{-9} to 1.5×10^{-6}	5×10^{-9}	Fluorescence	Hg^{2+}	40
Trp-GA-AgNPs	1×10^{-12} to 10×10^{-3}	0.658×10^{-12}	Fluorescence	Hg^{2+}	8
DNA-protected AgNPs	10×10^{-9} to 8×10^{-6}	2.6×10^{-9}	Fluorescence	Hg^{2+}	5
ss-DNA-templated AgNCs	$0–150 \times 10^{-9}$	4.5×10^{-9}	Fluorescence	Hg^{2+}	41
Polymethacrylic acid-AgNPs	$10–20 \times 10^{-9}$	10×10^{-9}	Fluorescence	Hg^{2+}	42
Citrate-AgNPs		90×10^{-9}	SERS	Hg^{2+}	43
4-Mercaptopyridine-AgNPs	$1–100 \times 10^{-9}$	0.34×10^{-9}	SERS	Hg^{2+}	44
Capped silver nanoprism	$0.5–100 \times 10^{-6}$	1.5×10^{-6}	UV-Vis	Hg^{2+}	45
Cellulose filter paper AgNPs		5 ppb	UV-Vis	Hg^{2+}	46
Unmodified AgNPs	0.01–10 mg L^{-1}	0.007 mg L^{-1}	UV-Vis	Hg^{2+}	47
Present study	3×10^{-9} to 13×10^{-6}	2.1×10^{-9}	UV-Vis, fluorescence	Hg^{2+}	
Epigallocatechin gallate-AgNPs	$1–10 \times 10^{-6}$	1.62×10^{-6}	UV-Vis	S^{2-}	18
BSA-AuNCs	$0.1–30 \times 10^{-6}$	0.029×10^{-6}	Fluorescence	S^{2-}	48
CNPs-AuNCs	$0–53 \times 10^{-6}$	18×10^{-9}	Fluorescence	S^{2-}	20
Chitosan capped-AgNPs	$0.8–6.4 \times 10^{-6}$	0.35×10^{-9}	UV-Vis	S^{2-}	49
Yeast extract-CuNCs	$0.02–0.8 \times 10^{-9}$	10×10^{-9}	Fluorescence	S^{2-}	26
DNA-Au/AgNCs	$0.01–9 \times 10^{-6}$	0.83×10^{-9}	Fluorescence	S^{2-}	50
Cysteine-CuNCs	$0.2–50 \times 10^{-6}$	42×10^{-9}	Fluorescence	S^{2-}	51
Present work	$3–170 \times 10^{-6}$	1.3×10^{-6}	Fluorescence	S^{2-}	
BSA-protected AuNCs	$0.3–20 \times 10^{-6}$	0.19×10^{-6}	Fluorescence	MG	52
CdTe/CdS quantum dots	$0.05–10 \times 10^{-6}$	0.029×10^{-6}	Fluorescence	MG	27
Molecularly imprinted mesoporous microspheres	27×10^{-9} to 137×10^{-6}	17×10^{-9}	Fluorescence	MG	53
Present study	$7–80 \times 10^{-6}$	1.6×10^{-6}	Fluorescence	MG	

the concentration of MG, thereby ruling out the possibility of interactions between the nanosensor and MG, which could be taken as an indication of the absence of the FRET mechanism. It has been reported that the quenching of fluorescence, which is caused by the absorbance of dyes with any covalent interaction between chromotropic receptors and fluorophore, is mainly attributed to inner filter effects.[35] Therefore the fluorescence of GA-AgNPs could be quenched by MG *via* the inner filter effect.[36]

3.12. Comparison of the performance of the developed nanosensor

The performance of our nanosensor towards Hg(II), S^{2-} and MG was compared with that of the other reported sensors (Table 1). It was found that our reported nanosensor showed satisfactory results in terms of sensitivity, performance, and detection limits.

3.13. Sensing of Hg(II), S^{2-} ions and MG in environmental samples

We tested our developed nanosensor to sense Hg(II), S^{2-} ions, and MG in environmental samples. Samples thus used were tap water, packaged drinking water (Bisleri), and borewell water. Hg(II), S^{2-} ions and malachite green were not detected in these samples. So, the respective samples were spiked with Hg(II), S^{2-} ions and malachite green at different concentrations, and the concentrations of Hg(II), S^{2-} and malachite green were tested by our proposed method, which was found to be in agreement with the spiked concentrations, and the recoveries for the samples

Table 2 Detection of Hg(II) in real environmental samples

Sample	Detected	Added (mol L^{-1})	Found (mol L^{-1})	Recovery (%)
Tap water	Not detected	50×10^{-9}	50.4×10^{-9}	100.8
		5×10^{-6}	5.05×10^{-6}	101
Borewell water	Not detected	50×10^{-9}	50.25×10^{-9}	100.5
		5×10^{-6}	5.02×10^{-6}	100.4
Bisleri	Not detected	50×10^{-9}	50.09×10^{-9}	100.2
		5×10^{-6}	5.01×10^{-6}	100.2

Table 3 Detection of S^{2-} in real environmental samples

Sample	Detected	Added (mol L^{-1})	Found (mol L^{-1})	Recovery (%)
Tap water	Not detected	10×10^{-6}	10.15×10^{-6}	101.5
		100×10^{-6}	100.4×10^{-6}	100.4
Borewell water	Not detected	10×10^{-6}	10.09×10^{-6}	100.9
		100×10^{-6}	100.16×10^{-6}	100.2
Bisleri	Not detected	10×10^{-6}	10.07×10^{-6}	100.7
		100×10^{-6}	100.08×10^{-6}	100.1

Table 4 Detection of MG in real environmental samples

Sample	Detected	Added (mol L^{-1})	Found (mol L^{-1})	Recovery (%)
Tap water	Not detected	50×10^{-6}	50.2×10^{-6}	100.4
		100×10^{-6}	100.5×10^{-6}	100.5
Borewell water	Not detected	50×10^{-6}	50.5×10^{-6}	101
		100×10^{-6}	100.7×10^{-6}	100.7
Bisleri	Not detected	50×10^{-6}	50.4×10^{-6}	100.8
		100×10^{-6}	100.6×10^{-6}	100.6

were statistically close to 100% (Tables 2–4), signifying that our proposed approach will prove to be useful in practical applications for the detection of Hg(II), S^{2-} ions and MG.

4. Conclusion

Stable and small-sized fluorescent silver nanoparticles were synthesized *via* a chemical reduction method utilizing a biocompatible natural polymer, *i.e.*, gum acacia as both a stabilizing and reducing agent. The dual (both colorimetric and fluorescence turn-on) response of the nanosensor towards Hg(II) ions was studied by noticing the changes in both the absorption and fluorescent features of the silver nanoparticles. The fluorescent features of the nanosensor were utilized for studying the sensing behavior towards S^{2-} ions and MG in 100% an aqueous medium. The developed nanosensor was also found to be useful in detecting the respective analytes in environmental samples.

Conflicts of interest

There are no conflicts to declare.

Acknowledgements

The Chairman, Department of Chemistry, Aligarh Muslim University, Aligarh, India, is acknowledged for providing the necessary research facilities to the department under SAP-DRS-II PURSE and FIST programs University Sophisticated Instruments Facility (USIF), Aligarh Muslim University, Aligarh, India, is acknowledged for providing TEM, SEM, and Confocal imaging facilities.

References

1 M. Annadhasan and N. Rajendiran, *RSC Adv.*, 2015, **5**, 94513–94518.
2 L. Rastogi, R. B. Sashidhar, D. Karunasagar and J. Arunachalam, *Talanta*, 2014, **118**, 111–117.
3 M. Sebastian, A. Aravind and B. Mathew, *Nanotechnology*, 2018, **29**, 355502.
4 L. Bell, J. DiGangi and J. Weinberg, *Ipen*, 2014, 1–209.
5 L. Deng, X. Ouyang, J. Jin, C. Ma, Y. Jiang, J. Zheng, J. Li, Y. Li, W. Tan and R. Yang, *Anal. Chem.*, 2013, **85**, 8594–8600.
6 S. K. Kailasa, M. Chandel, V. N. Mehta and T. J. Park, *Spectrochim. Acta, Part A*, 2018, **195**, 120–127.
7 P. K. Sarkar, N. Polley, S. Chakrabarti, P. Lemmens and S. K. Pal, *ACS Sens.*, 2016, **1**, 789–797.
8 P. Bian, L. Xing, Z. Liu and Z. Ma, *Sens. Actuators, B*, 2014, **203**, 252–257.
9 K. D. Bhatt, D. J. Vyas, B. A. Makwana, S. M. Darjee, V. K. Jain and H. Shah, *Chin. Chem. Lett.*, 2016, **27**, 731–737.
10 P. Vasileva, T. Alexandrova and I. Karadjova, *J. Chem.*, 2017, 1–9.
11 L. Qin, G. Zeng, C. Lai, D. Huang, C. Zhang, P. Xu, T. Hu, X. Liu, M. Cheng, Y. Liu, L. Hu and Y. Zhou, *Sens. Actuators, B*, 2017, **243**, 946–954.
12 L. Qin, H. Yi, G. Zeng, C. Lai, D. Huang, P. Xu, Y. Fu, J. He, B. Li, C. Zhang, M. Cheng, H. Wang and X. Liu, *J. Hazard. Mater.*, 2019, **380**, 120864.
13 Y. Fu, L. Qin, D. Huang, G. Zeng, C. Lai, B. Li, J. He, H. Yi, M. Zhang, M. Cheng and X. Wen, *Appl. Catal., B*, 2019, **255**, 117740.
14 P. Buduru, B. C. S. R. Reddy and N. V. S. Naidu, *Sens. Actuators, B*, 2017, **244**, 972–982.
15 A. Nain, S. R. Barman, S. Jain, A. Mukherjee and J. Satija, *Appl. Nanosci.*, 2017, **7**, 299–307.
16 S. Manivannan, Y. Seo, D. K. Kang and K. Kim, *New J. Chem.*, 2018, **42**, 20007–20014.
17 P. Prosposito, L. Burratti, A. Bellingeri, G. Protano, C. Faleri, I. Corsi, C. Battocchio, G. Iucci, L. Tortora, V. Secchi, S. Franchi and I. Venditti, *Nanomaterials*, 2019, **9**, 1–16.
18 R. K. Singh, B. Panigrahi, S. Mishra, B. Das, R. Jayabalan, P. K. Parhi and D. Mandal, *J. Mol. Liq.*, 2018, **269**, 269–277.
19 Y. Yan, K. Zhang, H. Yu, H. Zhu, M. Sun, T. Hayat, A. Alsaedi and S. Wang, *Talanta*, 2017, **174**, 387–393.
20 M. Liang, Y. Chen, H. Zhang, X. Niu, L. Xu, C. Ren and X. Chen, *Analyst*, 2015, **140**, 6711–6719.
21 T. S. Bailey and M. D. Pluth, *J. Am. Chem. Soc.*, 2013, **135**, 16697–16704.
22 J. Zeng, M. Li, A. Liu, F. Feng, T. Zeng, W. Duan, M. Li, M. Gong, C. Y. Wen and Y. Yin, *Adv. Funct. Mater.*, 2018, **28**, 1–10.
23 D. R. Canterford, *Anal. Chem.*, 1973, **45**, 2414–2417.
24 E. A. Guenther, K. S. Johnson and K. H. Coale, *Anal. Chem.*, 2001, **73**, 3481–3487.
25 K. Sasakura, K. Hanaoka, N. Shibuya, Y. Mikami, Y. Kimura, T. Komatsu, T. Ueno, T. Terai, H. Kimura and T. Nagano, *J. Am. Chem. Soc.*, 2011, **133**, 18003–18005.
26 L. Jin, Z. Zhang, A. Tang, C. Li and Y. Shen, *Biosens. Bioelectron.*, 2016, **79**, 108–113.
27 Z. Lin, W. Li, Q. Chen and A. Peng, *Int. J. Polym. Anal. Charact.*, 2019, **24**, 121–131.
28 W. Gui, H. Wang, Y. Liu and Q. Ma, *Sens. Actuators, B*, 2018, **266**, 685–691.
29 C. Yu, M. Leng, M. Liu, Y. Yu, D. Liu and C. Wang, *CrystEngComm*, 2012, **14**, 3772–3777.
30 H. Xu and K. S. Suslick, *ACS Nano*, 2010, **4**, 3209–3214.
31 C. Dong, X. Zhang, H. Cai and C. Cao, *J. Mol. Liq.*, 2014, **196**, 135–141.

32 I. Chakraborty, T. Udayabhaskararao and T. Pradeep, *J. Hazard. Mater.*, 2012, **211–212**, 396–403.
33 Y. Liu, Z. Zhu, G. Liu, Z. Xu, S. M. Kuznicki and H. Zhang, *J. Phys. Chem. C*, 2011, **115**, 14591–14597.
34 H. Chen, A. Fang, L. He, Y. Zhang and S. Yao, *Talanta*, 2017, **164**, 580–587.
35 N. Shao, Y. Zhang, S. Cheung, R. Yang, W. Chan, T. Mo, K. Li and F. Liu, *Anal. Chem.*, 2005, **77**, 7294–7303.
36 A. Fang, Q. Long, Q. Wu, H. Li, Y. Zhang and S. Yao, *Talanta*, 2016, **148**, 129–134.
37 P. Buduru, B. C. S. Raja and N. V. S. Naidu, *Sens. Actuators, B*, 2017, **244**, 972–982.
38 M. L. Firdaus, I. Fitriani, S. Wyantuti, Y. W. Hartati, R. Khaydarov, J. A. Mcalister, H. Obata and T. Gamo, *Anal. Sci.*, 2017, **33**, 831–837.
39 P. G. Mahajan, N. C. Dige, B. D. Vanjare, A. Rehman, S. Ja and K. Hwan, *J. Lumin.*, 2019, **206**, 624–633.
40 W. Guo, J. Yuan and E. Wang, *Chem. Commun.*, 2009, 3395–3397.
41 C. Li and C. Wei, *Sens. Actuators, B*, 2017, **242**, 563–568.
42 J. Liu, X. Ren, X. Meng, Z. Fang and F. Tang, *Nanoscale*, 2013, **5**, 10022–10028.
43 W. Ren, C. Zhu and E. Wang, *Nanoscale*, 2012, **4**, 5902–5909.
44 L. Chen, N. Qi, X. Wang, L. Chen, H. You and J. Li, *RSC Adv.*, 2014, **4**, 15055–15060.
45 F. Tanvir, A. Yaqub, S. Tanvir, R. An and W. A. Anderson, *Materials*, 2019, **12**, 1–12.
46 M. Ismail, M. I. Khan, K. Akhtar, J. Seo, M. A. Khan, A. M. Asiri and S. B. Khan, *J. Mater. Sci. Mater. Electron.*, 2019, **30**, 7367–7383.
47 S. Puchum, R. Meelapsom, S. S. Muniandy, H. L. Lee, S. Pencharee, M. Amatatongchai, K. Suttisintong and P. Jarujamrus, *Int. J. Environ. Anal. Chem.*, 2019, **99**, 139–156.
48 M. L. Cui, J. M. Liu, X. X. Wang, L. P. Lin, L. Jiao, Z. Y. Zheng, L. H. Zhang and S. L. Jiang, *Sens. Actuators, B*, 2013, **188**, 53–58.
49 K. Shanmugaraj and M. Ilanchelian, *Microchim. Acta*, 2016, **183**, 1721–1728.
50 W.-Y. Chen, G.-Y. Lan and H.-T. Chang, *Anal. Chem.*, 2011, **83**, 9450–9455.
51 Z. Li, S. Guo and C. Lu, *Analyst*, 2015, **140**, 2719–2725.
52 Y. J. Ju, N. Li, S. G. Liu, L. Han, N. Xiao, H. Q. Luo and N. B. Li, *Sens. Actuators, B*, 2018, **275**, 244–250.
53 W. Gui, H. Wang, Y. Liu and Q. Ma, *Sens. Actuators, B*, 2018, **266**, 685–691.

